Supplementary information

Biomimetic proteolipid vesicles for targeting inflamed tissues

R. Molinaro, C. Corbo, J. O. Martinez, F. Taraballi, M. Evangelopoulos, S. Minardi, I.K. Yazdi, P. Zhao, E. De Rosa, M. Sherman, A. De Vita, N.E. Toledano Furman, X. Wang, A. Parodi, and E. Tasciotti

SUPPORTING MATERIAL CONTENT

- **Supplementary Figure 9** *In vitro* adhesion of liposomes and leukosomes in flow condition to a reconstructed endothelium.
- **Supplementary Figure 10** PCR analysis of the level expression of pro- and anti-inflammatory markers, and endothelial adhesion molecules.
- **Supplementary Figure 11**. Bioluminescence imaging of mice to confirm local inflammation.
- **Supplementary Figure 12** Particles' distribution into the ear at 1 and 24 h after systemic injection.
- **Supplementary Figure 13** In vitro mechanisms of adhesion of leukosomes after either LFA-1 or CD45 blocking in flow condition to a reconstructed endothelium made by HUVEC cells pretreated with TNFα.
- **Supplementary Figure 14** In vivo mechanisms of particles' adhesion to the inflamed endothelium.
- **Supplementary Figure 15** Biodistribution and pharmacokinetics study of liposomes and leukosomes after 24 h from i.v. injection.
- **Supplementary Figure 16** Macroscopic observation of inflamed ears.
- **Supplementary Figure 17** Liver and kidney functionality.

Supplementary methods

Assembly of leukosomes

Leukosomes were prepared using the thin layer evaporation (TLE) method[1]. Briefly, 1,2-dipalmitoyl-sn-glycero-3-phosphocholine (DPPC), 1,2-distearoyl-sn-glycero-3-phosphocholine (DSPC), 1,2-dioleoyl-sn-glycero-3-phosphocholine (DOPC), and cholesterol (Avanti Polar Lipids), 5:1:3:1 molar ratio, respectively, were dissolved in a chloroform:methanol mixture (3:1 v/v) and the solvent was then evaporated through a rotary evaporator (BÜCHI Labortechnik AG, Switzerland) to form a thin film. Films were hydrated with membrane proteins (1:300 protein-to-lipid ratio) dispersed in PBS or PBS alone to assemble leukosomes or conventional liposomes, respectively, by three cycles of heating at 45°C and vortexing, 3 minutes each. Lipid suspension was then extruded ten times through 200 nm pore-size cellulose acetate membranes at 45°C and the obtained unilamellar vesicles were then dialyzed overnight through 1000 KDa membranes (Spectrum Laboratories, Inc.) to eliminate raw material and unincorporated proteins. Final liposome and leukosome concentration was assessed after dialysis by measuring rhodamine fluorescence of a diluted sample in 0.1% Triton-X100. Leukosomes were stored at 4°C until use.

Physical characterization of leukosomes

Dynamic light scattering analysis

Vesicle's size and polydispersity index were determined through dynamic light scattering analysis using a Nanosizer ZS (Malvern Instruments) that permitted also to evaluate their surface charge. 20 μl of liposome and leukosome suspensions were diluted in bi-distilled water and seven measurements were performed with 20 runs each and the results averaged.

CryoEM analysis

For electron microscopy analysis, lipid vesicles were plunge-frozen on holey film grids (R2x2 Quantifoil®; Micro Tools GmbH, Jena, Germany) as previously reported[2]. We have used a 626 cryo-specimen holder (Gatan, Inc., Pleasanton, California) for imaging. Data were collected on a JEOL 2100 electron microscope. Images were recorded under low electron-dose conditions (~5 - 20 electrons/Å2) using a 4,096 x 4,096 pxl CCD camera (UltraScan 895, GATAN, Inc.) at nominal magnifications of 20,000x.

Atomic Force Microscopy (AFM) analysis

AFM images of the liposomes and leukosomes were collected in Scan Asyst ®mode by Multimode (Bruker, CA, USA) using single-beam silicon cantilever probes (Bruker MLCT: resonance frequency 10 KHz, nominal tip radius of curvature 10 nm, force constant of 0.04N/m). Data sets were subjected to a first-order flattening. The particles roughness (Ra), an arithmetic value that describes the absolute height of a surface in comparison to a two-dimensional plane represented by the average sample height was calculated using Nanoscope 6.13R1 software (Digital Instruments, NY, USA). Mean values from 60 random particles in 3 independent experiments are reported. In addition, we performed the quantitative analysis of the AFM force mapping in order to evaluate the relative particles' elasticity. This technique directly measures the elastic properties of different surfaces resulting in a complete elastic property map of heterogeneous samples. We prepared the samples as reported in the main text that entails a 0.1% APTES coating of mica surface in order to stabilize the nanoparticles (avoiding their collapse on mica surface) and we performed the AFM analysis. The Young's modulus measurement has been calculated on 3 different samples corresponding to 512 × 512 force–separation curves obtained over an area 10 μm × 10 μm.

The Young's elastic modulus was calculated using the following equation previously reported [3, 4]

$$F - F_{adh} = 4/3\ E^*\ \sqrt{R(d - d_0)}^3$$

Fourier Transform Infrared spectroscopy (FTIR) analysis

FTIR measurements in attenuated total reflection (ATR) were performed using a single reflection diamond element. The FTIR spectrometer Nicolet equipped with nitrogen cooled mercury cadmium telluride detector and an air purging system, was employed under the following conditions: 2 cm^{-1} spectral resolution, 20 kHz scan speed, 1000 scan co-addition, and triangular apodization. Each sample was dissolved at a final concentration of 1 mg ml^{-1} in PBS. 5 µl of each sample were deposited on the ATR plate and spectra were recorded after solvent evaporation to allow the formation of a hydrated lipid film. After these measurements, the same samples were re-suspended, and the spectra were recorded again after the solvent evaporation for three times in order to confirm the data. The ATR/FTIR spectra were reported after background subtraction and normalization on the C=O vibrational mode located at ≈1730 cm^{-1} band area to compensate for possible differences in the lipid content.

Differential scanning calorimetry (DSC) analysis

Leukosomes with different protein/lipid ratio (1:100, 1:300, 1:600) were prepared for DSC measurements using a Mettler-Toledo Star DSC (Mettler-Toledo, Switzerland). Liposomes were used as control, to evaluate differences in the bilayer thermal transitions with increasing protein content. A concentrated aqueous suspension of the samples was placed in an alumina pan for analysis, and an empty pan was used as reference. The heating scan was from 25 to 60 °C at the rate of 5 °C/min. DSC curves were analyzed using the fitting program.

Analysis of leukosome protein composition

Sample preparation and LC/MS^E conditions

Leukosomes were analyzed via peptide-level LC/MS^E analysis by in-solution trypsin digestion after reduction and alkylation of disulfide bridges as follows. Samples were resuspended with 0.5% RapiGest SF surfactant (Waters Corp, Milford, MA) in 50mM ammonium bicarbonate (AMBIC) at pH 8.0, and then treated with 5mM dithiothreitol (DTT) at 60°C for 30min, and with 15mM iodoacetamide (IAA) at room temperature in the dark. Samples were de-lipidated with methanol/chloroform extraction. Bradford (Bio-Rad) protein assay was employed to determine protein concentration, then trypsin digestions were performed overnight at 37°C (enzyme:substrate = 1:50 molar ratio). Reactions were stopped by changing the pH of the solution, and by adding 0.5% of trifluoroacetic acid. A Waters Corp. NanoAcquity UPLC system coupled with a Synapt HDMS (G1) mass spectrometer was employed. The peptide mixtures were separated with a reverse phase C-18 column and then injected into the mass spectrometer in positive ion (ESI) mode. The LC system consisted of a 180um x 20mm Symmetry C18 (5um particle) trapping column, and a 75um x 250mm BEH130 C18 (1.7um particle) analytical column. Peptide separation was carried out by a 3-40% gradient of solvent B (0.1% formic acid in acetonitrile) in solvent A (0.1% formic acid in water) over 120min at flow of 0.3ul/min and a column temperature of 35°C. The mass spectrometer was operated in the data independent (parallel-ion fragmentation) MS^E mode [5-7] at a capillary voltage of 3kV, with alternating low (6V) and ramped high collision energies (15V–45V) at a scan rate of 1.2sec per scan. The Glu-fibrinopeptide B (GFP) was sampled every 30secs as internal calibrant. All data was collected with the time of flight (TOF) detector set in the V-mode (resolution ~10,000). All LC/MS instrument control and data acquisition was accomplished using MassLynx (v4.1) software from Waters Corp. The samples were analyzed in triplicate.

Protein identification and classification

For protein identification and quantification we employed ProteinLynx Global Server (PLGS v2.4; Waters Corp) software, using both the IdentityE and ExpressionE algorithms included in the software. Precursor ions and fragment ion mass error tolerance levels (typically less than 5ppm and 15ppm respectively) were calculated automatically by the software. The Uniprot 2013_03 ('reviewed') (16,614 entries) complete mouse proteome database was interrogated. The false discovery rate (FDR) for protein identifications was set at 1%. Peptide identifications were accepted with a minimum of 2 peptides and 7 fragment ions matched per protein, with a minimum of 4 fragment ions per peptide detected. As database search parameters, we selected a) carbamidomethyl-cysteine as fixed modification, b) oxidized-methionine as variable modification, c) and one trypsin miscleavage. All protein identifications were further filtered to retain only those protein IDs that remained above the 95% confidence interval. The whole protein data set (Table) identified in the leukosomes was submitted to bioinformatics analysis and classified on the basis of biological process and cellular component. The proteins were classified according to UniProt/GO (http://www.uniprot.org/) (http://www.geneontology.org/) information and manually searching in literature.

Evaluation of protein orientation into leukosome bilayer

Flow cytometry analysis was performed to validate the presence of leukocyte-derived membrane proteins and to confirm their correct orientation into leukosome bilayer. Leukosomes and liposomes were diluted in FACS Buffer (PBS, 1% BSA) to a final concentration of 0.5 mM and incubated separately with FITC-labeled anti-Mac-1 and anti-LFA-1, PerCP-labeled anti-CD45, PE-labeled PSGL-1 and CD18, and AlexaFluor 647-labeled CD47 (2.5 μg/ml) designed to bind the protein's extracellular domain for at

least 30 min at room temperature. Samples were next dialyzed using 1000 kDa membrane filters for 1.5 h in water covered from light with mild stirring and then analyzed on the flow cytometer. The analysis was performed also after dexamethasone loading to verify whether drug encapsulation affects surface properties.

Characterization of protein glycosylation

Glycosylation of membrane-associated proteins was verified using the wheat germ agglutinin (WGA) assay (Life Technologies, San Diego, CA). WGA is a carbohydrate-binding protein that selectively binds N-acetyl-D-glucosamine and sialic acid glycosylated residues on the plasma membrane. Briefly, samples (liposomes, leukosomes and extracted and purified membrane proteins) were incubated at 1 μg/ml Alexa Fluor® 488-conjugated WGA in standard buffers (HBSS) for 10 minutes and then washed through dialysis. WGA fluorescence (excitation/emission maxima ~495/519 nm) was spectrofluorometrically measured.

Evaluation of *in vitro* adhesion ability of leukosomes to a reconstructed endothelium

Flow experiments were performed by seeding HUVEC cells onto ibidi μ-slide $I^{0.4}$ Luer ibiTreat, tissue culture treated slides. Briefly, slides were incubated for 1 h to equilibrate slides followed by 30 min incubation with fibronectin at a concentration of 50 μg ml^{-1}. HUVEC were then seeded at 1.25 × 10^6 cell ml^{-1} and incubated for 24 h. Slides were then washed by slowly passing PBS into the wells. Rhodamine-labeled Leukosomes and liposomes, resuspended in EBM-2 media, were then infused into the slides using a Harvard Apparatus PHD 2000 Infusion syringe pump at a speed of 100 μl min^{-1} for 30 min. In order to investigate the mechanism of adhesion of leukosomes, either LFA-1 or CD45 were blocked on leukosome surface as indicated in the previous paragraph

(**Evaluation of protein orientation into leukosome bilayer).** After infusion was complete, cells were briefly washed in PBS then fixed for 10 min using 4% paraformaldehyde at room temperature. Nucleus was then stained by infusing cells for 1 min with a PBS solution containing 4',6-diamidino-2-phenylindole (DAPI) then washed to remove any free DAPI. Cells were then left in PBS and immediately images using an inverted Nikon Eclipse Ti fluorescence microscope equipped with a Hamamatsu ORCA-Flash 2.8 digital camera.

***In vivo* experiments**

All animal experiments were performed in accordance with the guidelines of the Animal Welfare Act and the Guide for the Care and Use of Laboratory Animals approved by The Houston Methodist Institutional Animal Care and Use Committee guidelines (Houston, TX).

Ear inflammation was generated in Balb/c mice (Charles River Laboratories, Wilmington, MA) by a one-time injection of LPS (10 μg) in the right ear. Particles were administrated 30 minutes after LPS injection. Mice were prepared for intravital microscopy imaging at 1 and 24 h after particles injection to assess their targeting and distribution (vascular vs extravascular space).

Histology of ear tissue

Explanted Mice ears were washed twice with PBS and embedded in a cryomold in O.C.T. (Tissue-Tek® O.C.T. Compound, Sakura® Finetek), and instantly frozen at -80 degree. Ten μm-thick slides were obtained cutting ears block with a cryostat at -20 degree. The slides were then stored at -20 degree until the analysis.

Intravital experiments

Imaging of particle accumulation in ear

Anesthetized animals were placed and imaged on an upright Nikon A1R MP-ready laser scanning intravital confocal microscopy (IVM) platform equipped with a resonance scanner, isoflurane anesthesia system, heated stage, and custom coverslip mounts. Before imaging, a bolus injection of 70 kDa FITC-dextran (50 µL in PBS) was used to delineate the vasculature. Images were obtained with a three-channel setup in which fluorescence was collected at 488/525 nm for FITC dextran, and at 561/579 nm for rhodamine-labeled particles. Image acquisition was performed over selected field of views (FOVs) with resolution of 512 x 256 pixels with an optical slice thickness of 7.1 µm. Imaging to determine extent of leukosomes was performed 1 h and 24 h after the initial *i.v.* injection (50 µL, 1 mg/mL).

Image analyses and particle quantification

The average number of particles (leukosomes or liposomes) preferentially accumulated in ear microenvironment was enumerated in video stills using Nikon NIS element AR software (Nikon, Mellville, NY). Select FOVs were chosen from time-lapse videos and automated object measurement feature was used to calculate area fraction fluorescent particles in each frame where a particle was defined by setting low and high pixel thresholds to include only visible red fluorescent particles and to exclude single noise pixels. The settings were applied to all frames and automated counting function used to generate average area fraction of particles for each time point. These settings were also kept constant across treatment groups. The average area fraction covered by fluorescent particles was normalized to the imaging area and then plotted as a function of time.

Biodistribution and pharmacokinetic profile of leukosomes

Balb/c mice were i.v. injected with 2 mg of rhodamine-labeled liposomes and leukosomes (n=5 for each group) in order to evaluate particle biodistribution and pharmacokinetic profile. After 24 h, mice were sacrificed and major organs (kidney, liver, kidney, and lung) and ear tissue were collected, washed twice with PBS, weighted and transferred in a falcon tube. Tubes were then filled with formamide (1 ml per 100 mg of tissue weight) and tissues were homogenized. After 2 h of incubation at room temperature, samples were centrifuged at 5,000 g per 10 min and supernatant was collected and spectrofluorometrically analyzed for rhodamine detection (excitation/emission 561/579; slit width, 5 nm). Results are represented as relative signal per organ (%) based on a standard curve to calibrate rhodamine-labeled phospholipid.

For pharmacokinetic studies, blood was collected from the retro orbital plexus (n=5 for each group) at 24 h after injection, and centrifuged at 1,500 rpm for 10 min to isolate plasma. Rhodamine concentration was measured based on fluorescence and calculated as aforementioned.

Bioluminescence imaging of lipopolysaccharide-induced acute ear inflammation

Bioluminescence imaging of mice was used to confirm local inflammation. The right ears of mice were inflamed with a subcutaneous injection of 10 µL of LPS. Mice were imaged for bioluminescence (BLI) 5 min after i.p. administration of 5 mg (250-300 mg/kg) of luminol (Sigma Aldrich) for 5 min at medium binning and an f/stop of 1 on a IVIS Spectrum. Luminol is a small molecule that enables noninvasive bioluminescence imaging of myeloperoxidase[8] (an enzyme found only in activated phagocytes, such as neutrophils). Images were analyzed using the Living Image Software and the average radiance in both ears was collected.

Statistical analysis

GraphPad statistical software (La Jolla, CA) was used to compute statistical significance between groups and control using student's test and one-way ANOVA test to compare differences between groups. A value of $p = 0.05$ was considered statistically significant. Intravital microscopy data are presented as means ± standard deviation obtained from at least 10 field of views (FOVs) for n = 3. The allocation of the animals to the different groups of treatment was at random. To diminish the occurrence of bias, the experiments were done "blind".

Supplementary Figures

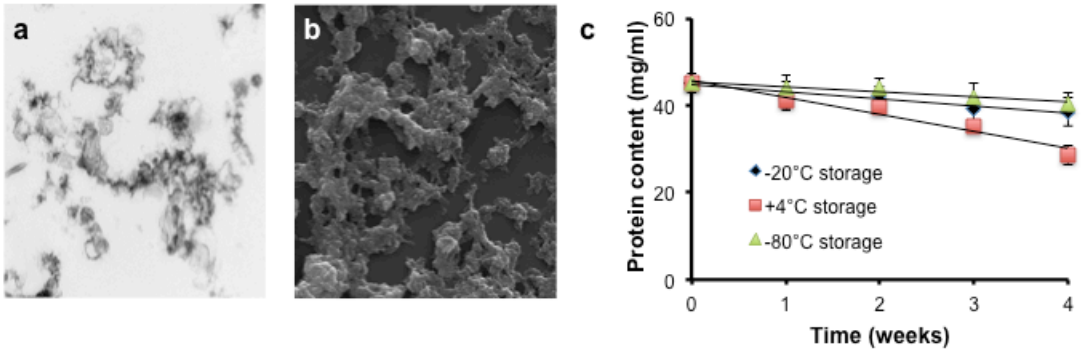

Figure 1 EM micrographs of leukocyte-derived membranes and storage stability of extracted membrane proteins. **a,** TEM and **b,** SEM images of purified leukocyte membranes; **c**, storage stability of membrane proteins evaluated as content of total proteins over 4 weeks storage at different temperatures.

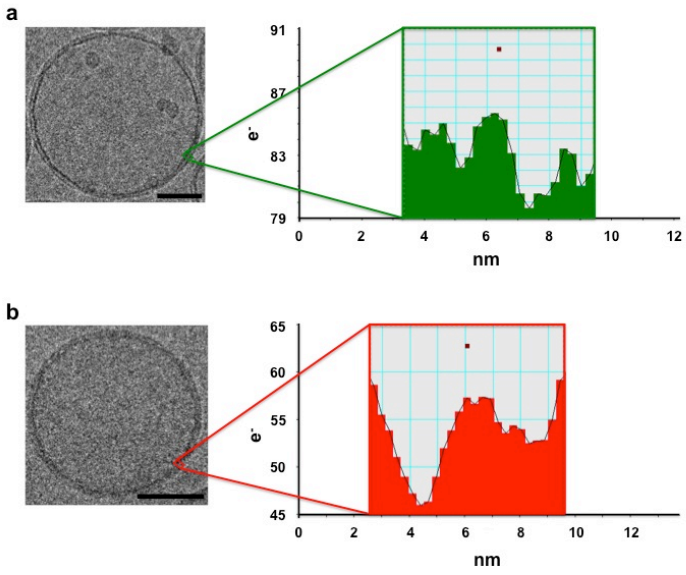

Figure 2 High-magnification cryo-TEM images of a liposomal (**a**) and a leukosomal (**b**) vesicle are shown along with corresponding line profiles through lipid bilayers. The vesicles were selected from pictures of both types of cryo-TEM samples taken with similar defocus values to ensure comparable imaging conditions. The analysis reveals a slight, but significant thicker bilayer for leukosomes with respect to liposomes. Scale bar = 50 nm.

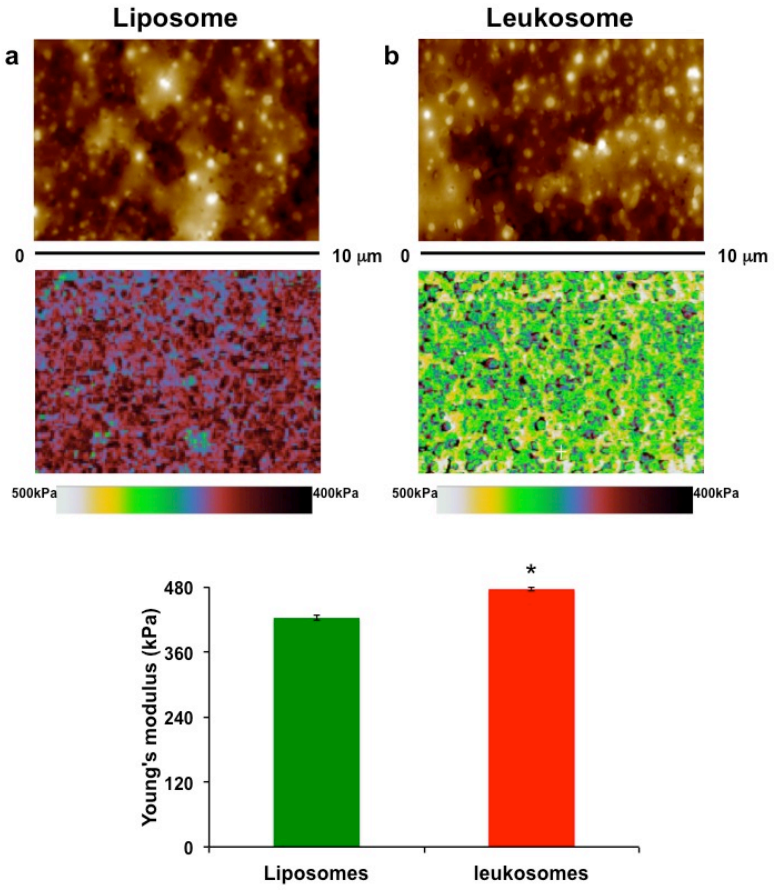

Figure 3 Heights representation and property map of Young's modulus of a representative sample of liposome (**a**) and leukosome (**b**) images using AFM analysis. The elastic modulus for leukosomes (476 kPa) resulted slightly but significantly increased with respect to the one for liposomes (423 kPa). The increase in the Young's modulus corresponds to a higher stiffness of the leukosomes' bilayer compared to the liposomal one.

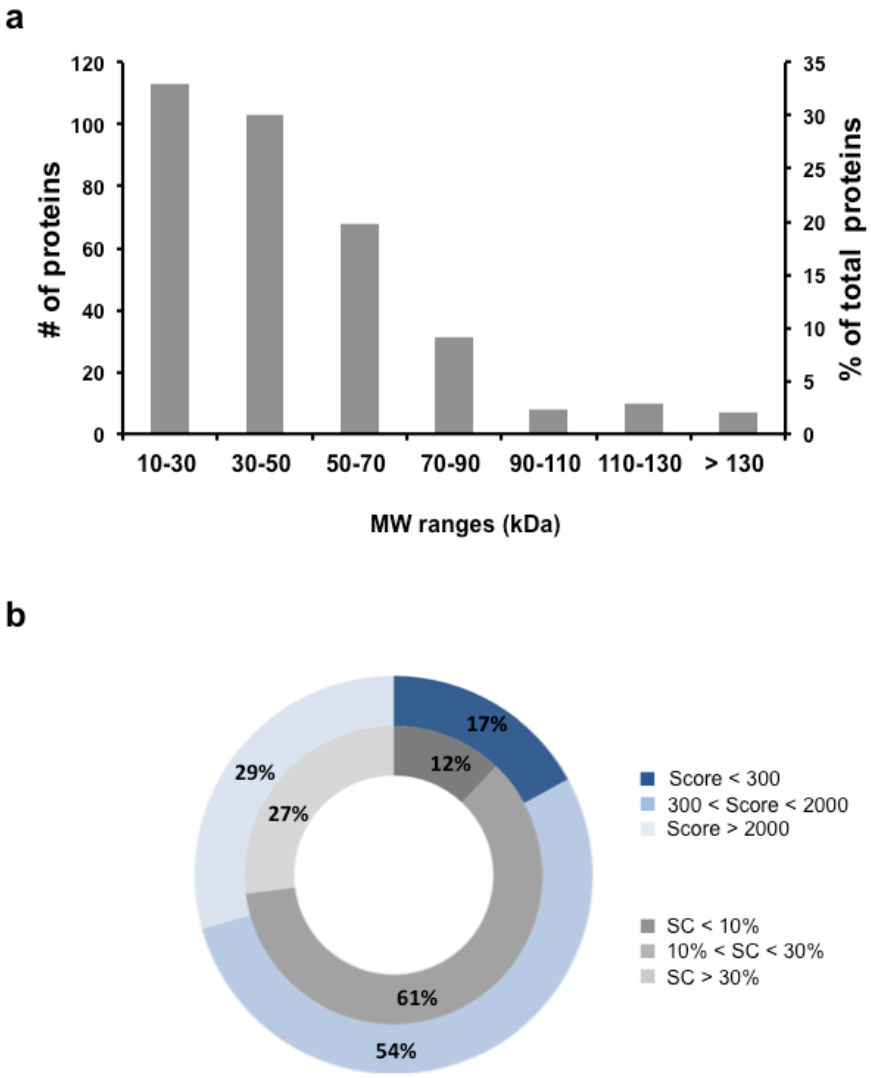

Figure 4 Molecular weights (MW) and Score and Sequence Coverage (SC) distribution of the proteins identified in the leukosomes. **a**, Molecular weights (MW) distribution of the proteins identified in the leukosomes. The number of proteins falling into each MW range is plotted on the left y-axis, while the percentage of proteins is showed on the right y-axis. **b, Score and Sequence Coverage (SC) distribution.** Proteins classification according to their Score (blue scale) and Sequence Coverage (grey scale) obtained by mass spectrometry analysis. Distribution analysis reveals that most of the proteins have been identified with a score in the range 300-2000 and a sequence coverage between 10 and 30%.

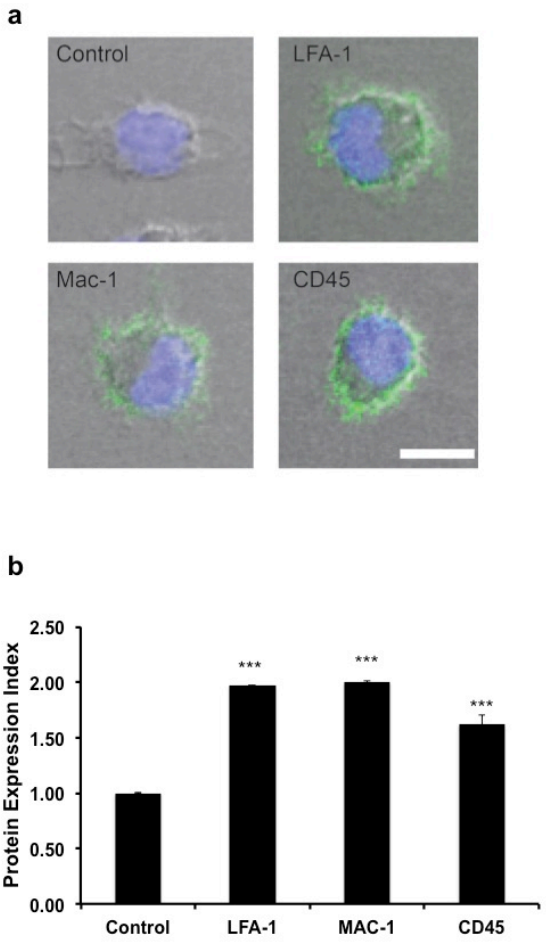

Figure 5 Validation of markers' expression on J774 surface a, Immunofluorescence analysis of J774 macrophages stained with FITC-labeled anti-LFA-1, anti-MAC-1, and anti-CD45; **b**, Flow cytometry analysis validates LFA-1, CD45 and Mac-1 presence and their correct orientation on the surface of J774 macrophage. ***p<0.001.

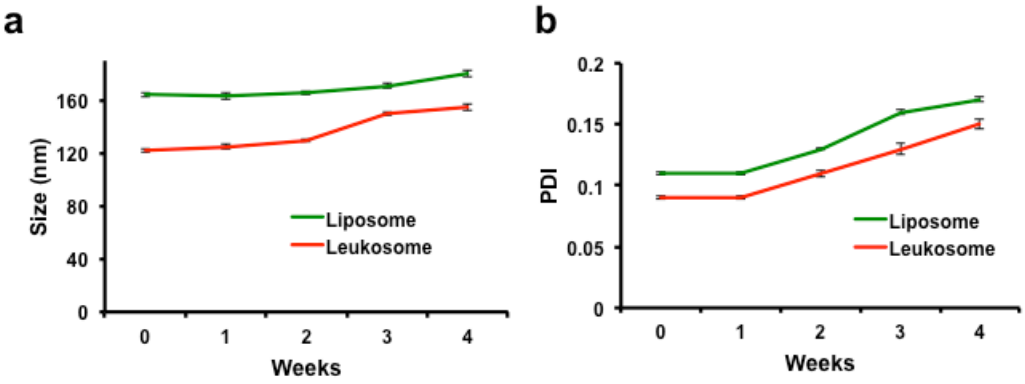

Figure 6 Storage stability of liposomes and leukosomes at 4°C was evaluated by DLS analysis. Average size (**a**) and polydispersity index (PDI) (**b**) were measured up to 4 weeks from assembly.

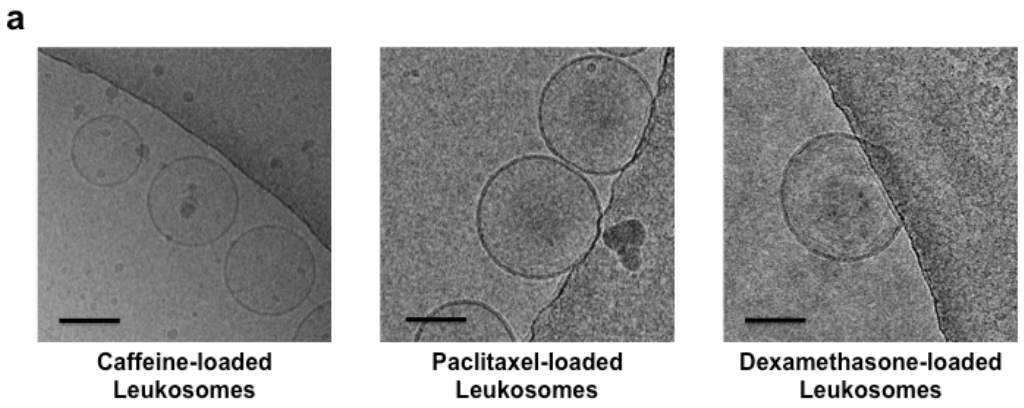

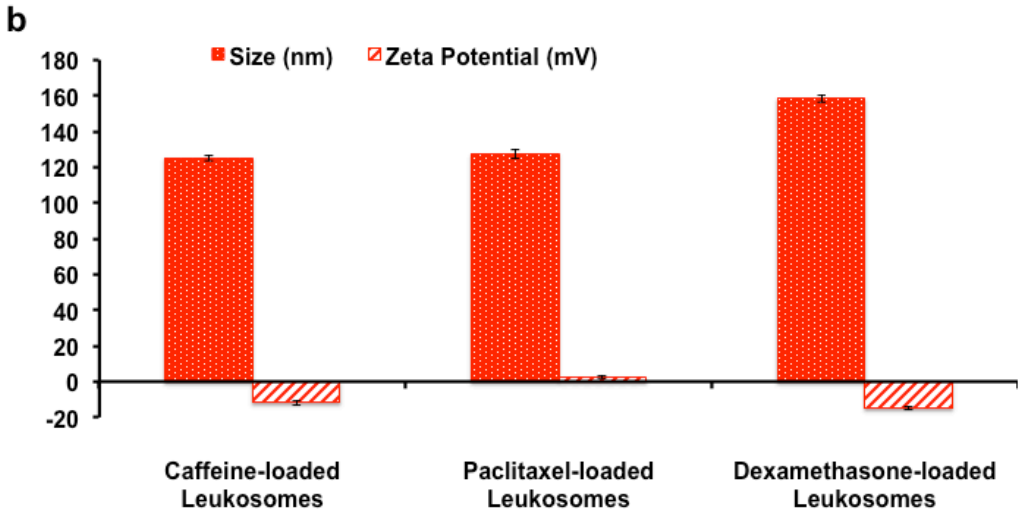

FORMULATION	PDI	SD (±)
Caffeine-loaded Leukosome	0.07	0.003
Paclitaxel-loaded Leukosome	0.1	0.012
Dexamethasone-loaded Leukosome	0.05	0.017

Figure 7 Physical characterization of drug-loaded leukosomes. **a,** cryoEM analysis of caffeine, paclitaxel, and dexamethasone-loaded leukosomes shows vesicular structure and spherical shape typical of empty vesicles. **b** DLS analysis revealed that caffeine, paclitaxel, and dexamethasone did not significantly affect leukosome physical properties (size and formulation homogeneity). A significant change in zeta potential values can be noted after paclitaxel encapsulation. PDI: polydispersity index.

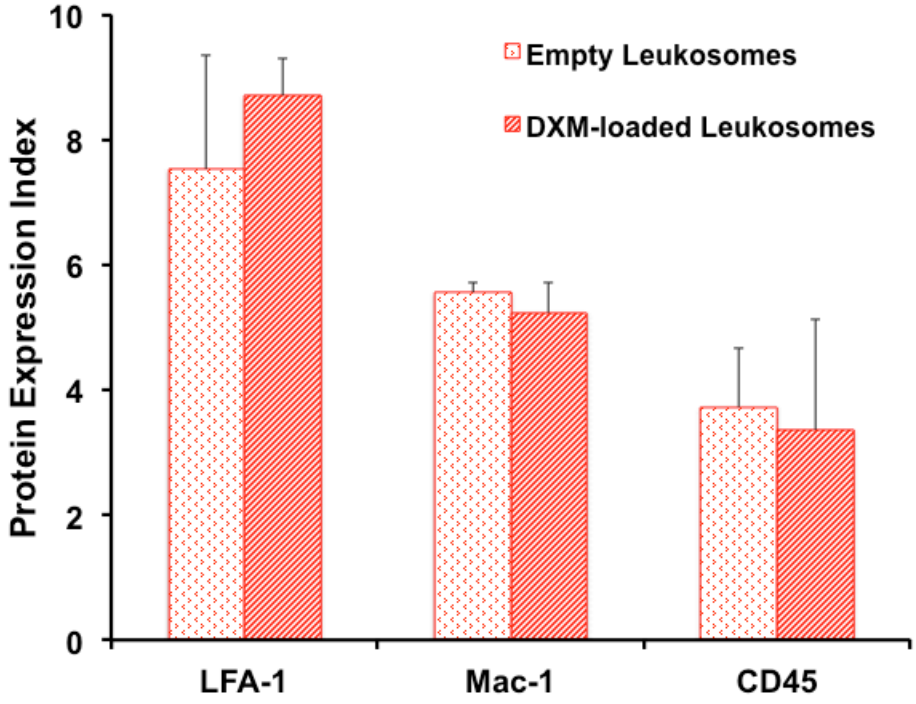

Figure 8 Marker's expression on leukosome surface after drug loading. Dexamethasone (DXM) encapsulation did not affect the surface properties of leukosome. LFA-1, Mac-1, and CD45 presence and correct orientation on carrier's surface was evaluated through flow cytometry analysis of dexamethasone (DXM) -loaded leukosomes as above described. Each result is the average of 5 different measurements ± SD.

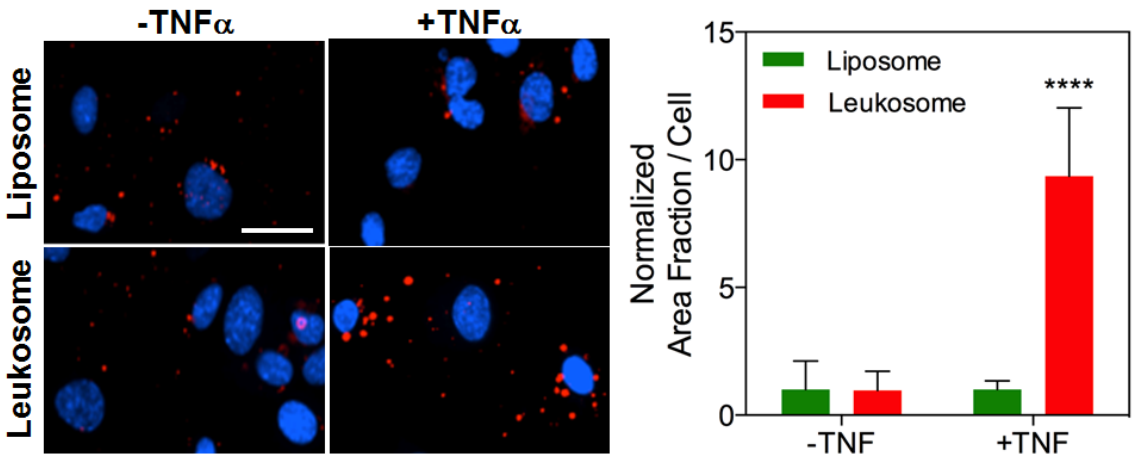

Figure 9 *In vitro* adhesion of liposomes and leukosomes in flow condition to a reconstructed endothelium made by HUVEC cells. No statistically significant difference in adhesion was found between liposomes and leukosomes in not inflamed conditions, while after pre-treatment of HUVEC cells with TNFα, leukosome targeting was significantly higher than liposomes. ****p<0.0001. Scale bar = 25 μm.

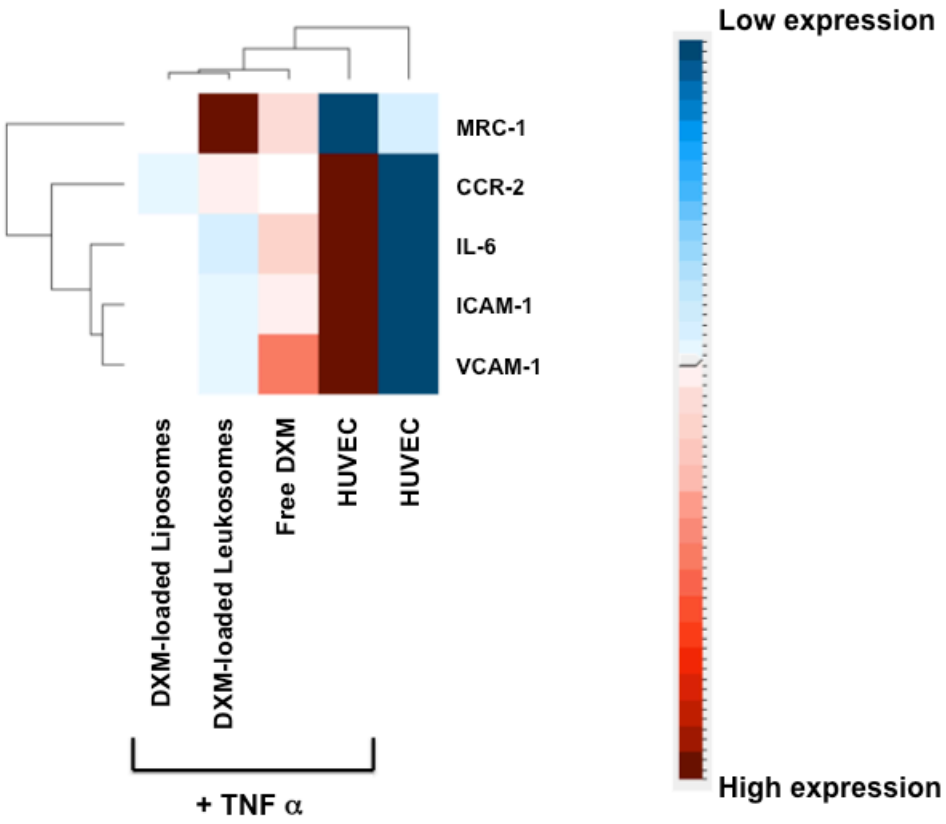

Figure 10 PCR analysis of pro (CCR-2, and IL-6), anti (MRC-1)-inflammatory markers, and endothelial adhesion molecules (ICAM-1 and VCAM-1) expression. Heat map study shows how leukosomes were significantly more efficient than DXM free ($p<0.001$) and loaded into liposomes ($p<0.01$) in reducing the expression of pro-inflammatory genes and of the adhesion molecules ICAM1 and VCAM1, typically over-expressed in case of vascular inflammation and responsible of the subsequent leukocytes' binding. In addition, MRC-1 gene levels resulted increased after leukosome treatment compared to free and liposome-loaded DXM ($p<0.001$).

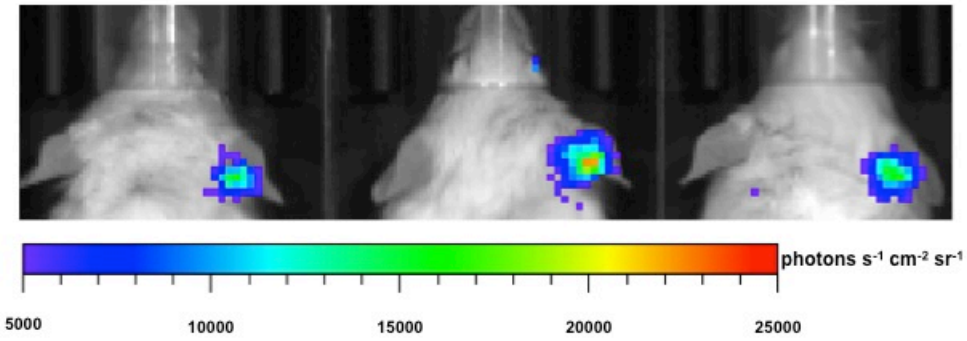

Figure 11. Bioluminescence imaging of mice to confirm local inflammation. 24 hours after administration of LPS on the left ears of mice, Mice were treated with 5 mg/mouse of luminol. BLI analysis shows luminol signals originating only from the right ear while the left ear (control) had negligible signal. This imaging confirmed that inflammation was restricted to the right ears with prominent recruitment of neutrophils.

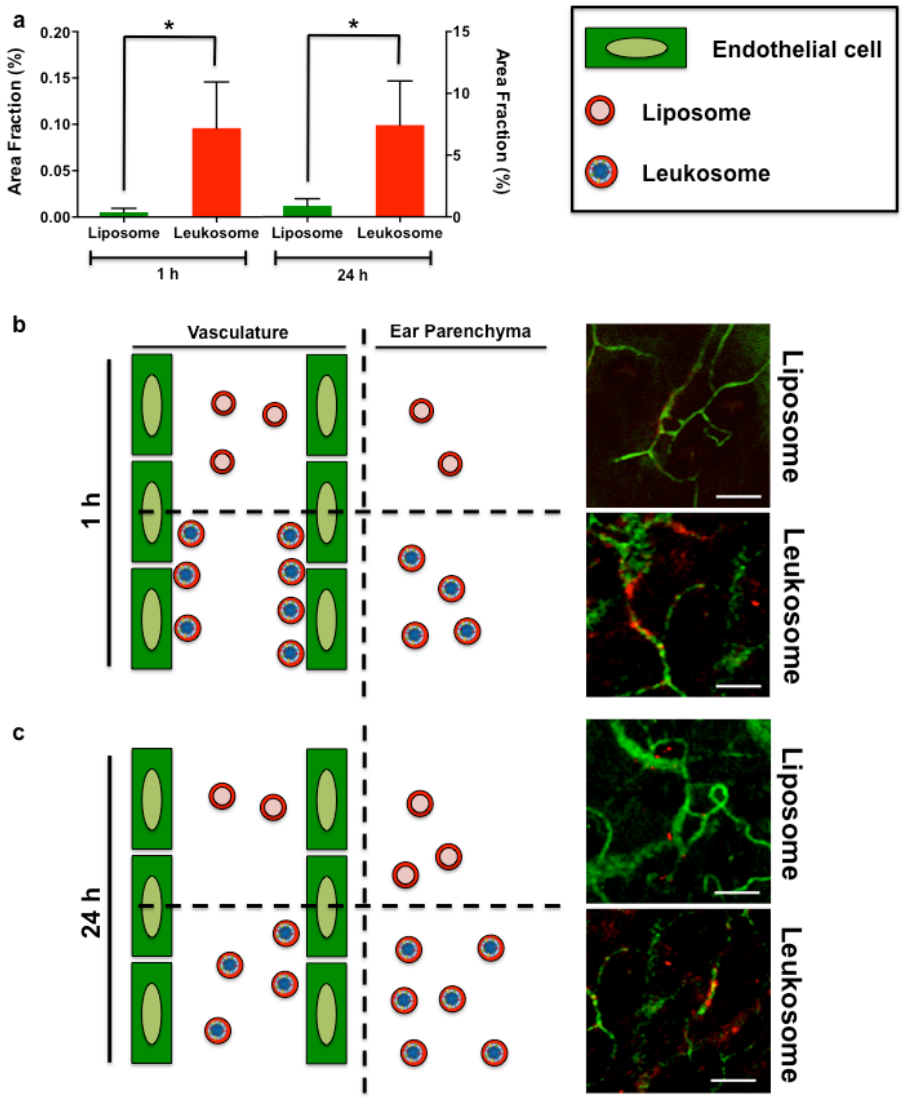

Figure 12 Particles' distribution into the ear at 1 and 24 h after systemic injection. **a**, Liposomes and leukosomes accumulation into the inflamed ear tissue at 1 and 24 h after injection. **b**, Liposomes are more abundant into the extravascular space at 1 h, as a result of the EPR effect occurring at the vascular level following the LPS-induced inflammation, while leukosomes are associated to the vasculature, due to their active-targeting properties. **c**, At 24 h, liposomes are in equilibrium between the two environments, while leukosomes gradually crossed the vascular barrier accumulating into the extravascular space. Scale bar = 50 μm.

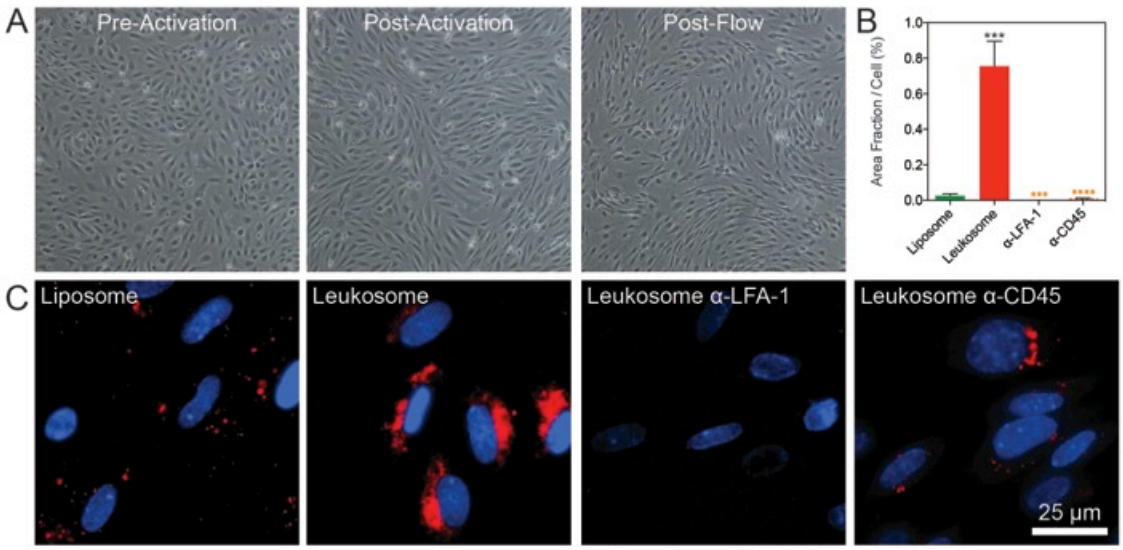

Figure 13 In vitro mechanisms of adhesion of leukosomes after either LFA-1 or CD45 blocking in flow condition to a reconstructed endothelium made by HUVEC cells pretreated with TNFα. Compare to control leukosomes, a significant reduction of particles' adhesion can be observed after blocking of either LFA-1 (α-LFA-1) and CD45 (α-CD45) on leukosome surface, thus confirming that the adhesion is mainly regulated by LFA-1, and validating the cooperative effect between these two markers. ***p<0.005; ****p<0.001. Stars represent relative to liposome. Dots represent relative to Leukosome.

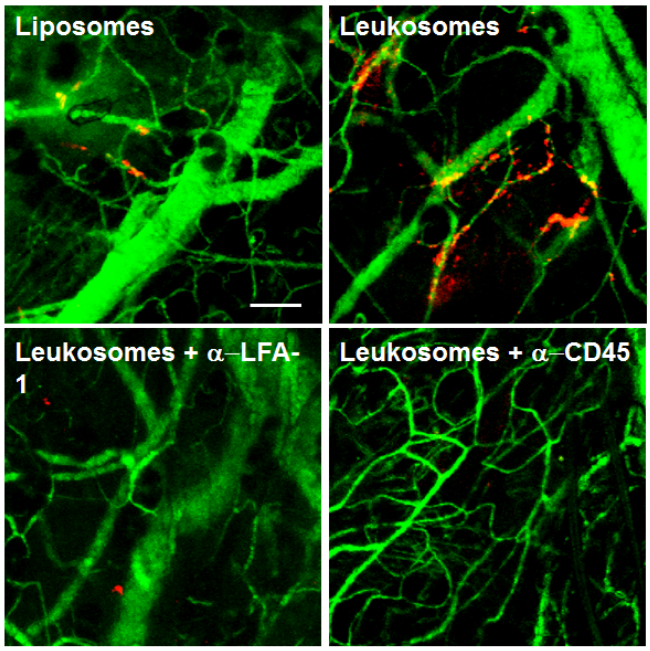

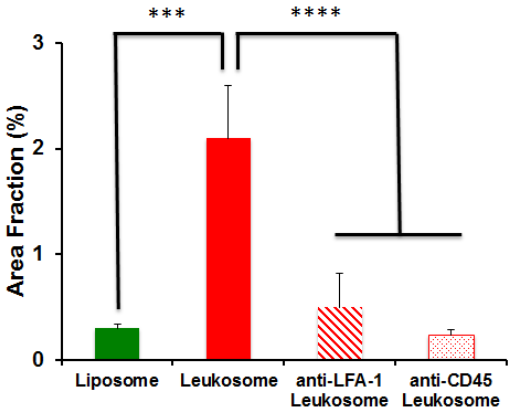

Figure 14 *In vivo* mechanisms of particles' adhesion to the inflamed endothelium. The figure shows the targeting abilities of leukosomes toward LPS-inflamed ear after blocking of either LFA-1 or CD45 on their surface. The blocking of either LFA-1 or CD45 nullifies the targeting abilities of leukosomes, which, as a result, show a significantly reduced adhesion with respect to the control leukosomes. In addition, no statistically significant difference can be observed among anti-LFA-1, or anti-CD45-leukosomes and liposomes, thus indicating that, after blocking, the only mechanism of accumulation remains the passive targeting. ***p<0.001; ****p<0.0001. Scale bar = 50 μm.

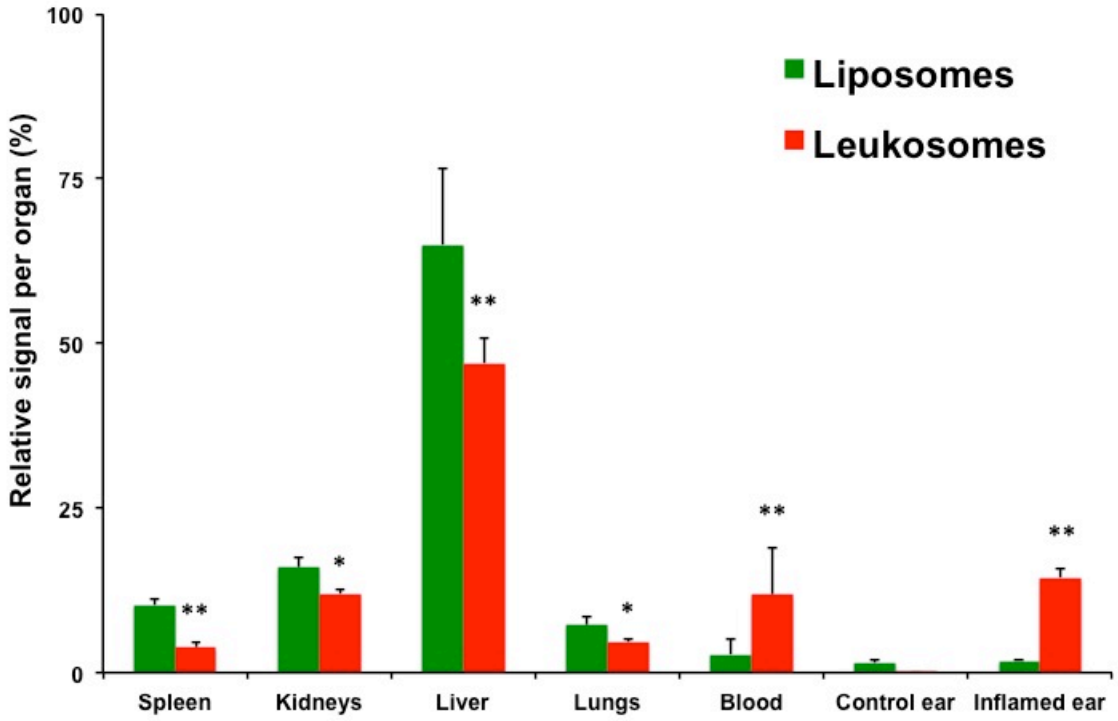

Figure 15 Biodistribution and pharmacokinetics study of liposomes and leukosomes after 24 h from i.v. injection. Mice (n=5 for each group) received 2 mg of rhodamine-labeled liposomes and leukosomes. 30 µl blood was collected from the retro orbital plexus at the time points and the rhodamine-related fluorescence was quantified for fluorescence.

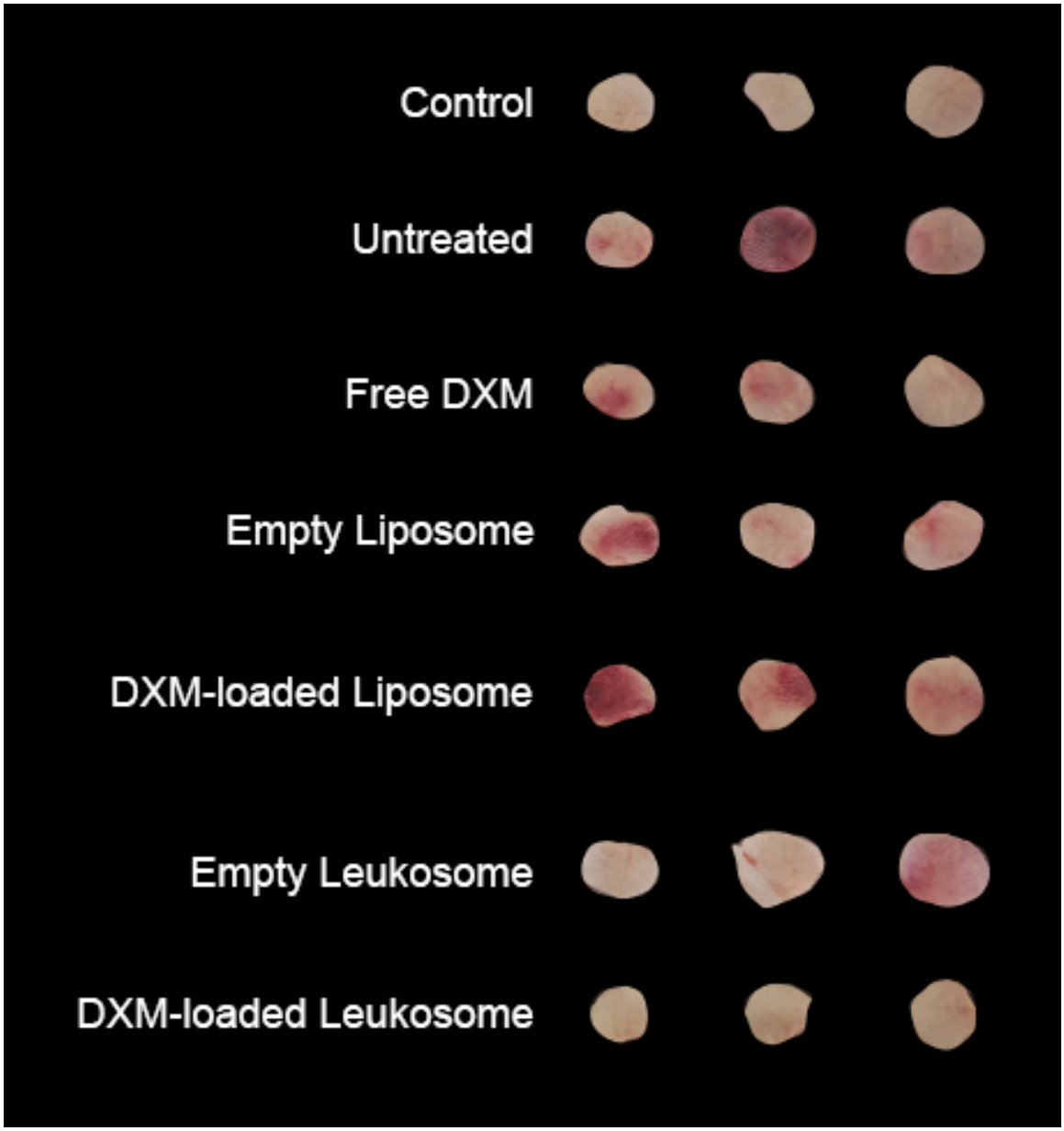

Figure 16 Macroscopic observation of inflamed ears. Representative left (control) and right (treated) ears of mice (n=3) were harvested and punched. Macroscopic observation revealed the classical signs of inflammation, calor, rubor, and tumor (heat, redness, and swelling), clearly visible by eye, and further macroscopically investigated.

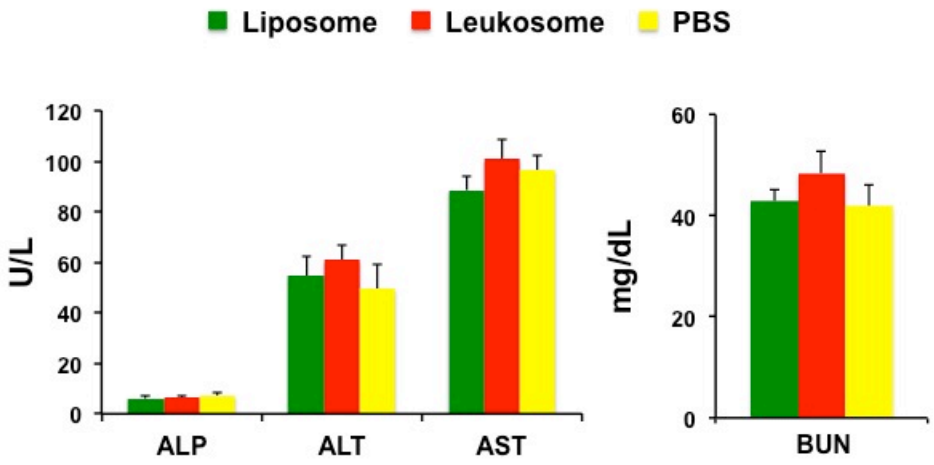

Figure 17 Liver and kidney functionality. Blood test parameters after administration of leukosomes, liposomes and PBS (mean ± SD, n = 3) revealed how leukosomes did not induce any change in liver (ALP, ALT, and AST) and kidney (BUN) functionality with respect to PBS and liposome groups.

References

1. Laouini, A. et al. Preparation, characterization and applications of liposomes: state of the art. *Journal of Colloid Science and Biotechnology* **1**, 147-168 (2012).
2. Sherman, M.B. et al. Removal of divalent cations induces structural transitions in red clover necrotic mosaic virus, revealing a potential mechanism for RNA release. *Journal of virology* **80**, 10395-10406 (2006).
3. Ramachandran, S., Quist, A.P., Kumar, S. & Lal, R. Cisplatin nanoliposomes for cancer therapy: AFM and fluorescence imaging of cisplatin encapsulation, stability, cellular uptake, and toxicity. *Langmuir* **22**, 8156-8162 (2006).
4. Minardi, S. et al. Evaluation of the osteoinductive potential of a bio-inspired scaffold mimicking the osteogenic niche, for bone augmentation. *Biomaterials* (2015).
5. Silva, J.C. et al. Quantitative proteomic analysis by accurate mass retention time pairs. *Analytical chemistry* **77**, 2187-2200 (2005).
6. Silva, J.C., Gorenstein, M.V., Li, G.-Z., Vissers, J.P. & Geromanos, S.J. Absolute quantification of proteins by LCMSE a virtue of parallel MS acquisition. *Molecular & Cellular Proteomics* **5**, 144-156 (2006).
7. Geromanos, S.J. et al. The detection, correlation, and comparison of peptide precursor and product ions from data independent LC‐MS with data dependant LC‐MS/MS. *Proteomics* **9**, 1683-1695 (2009).

8. Gross, S. et al. Bioluminescence imaging of myeloperoxidase activity in vivo. *Nature medicine* **15**, 455-461 (2009).